frontiers | Frontiers in Earth Science

ORIGINAL RESEARCH
published: 06 April 2022
doi: 10.3389/feart.2022.849041

Biomarker Records From Eocene Lacustrine Sequence in the Eastern Tibet Plateau and Its Implication for Organic Matter Sources

Jingyi Wei[1,2], Yongli Wang[1], Gen Wang[3]*, Zhifu Wei[3], Wei He[3], Ting Zhang[3], Xueyun Ma[3,2], Pengyuan Zhang[1,2], He Ma[1,2], Xiaoli Yu[3,2], Shangkun Li[3,2] and Lun Li[3,2]*

[1]*Key Laboratory of Cenozoic Geology and Environment, Institute of Geology and Geophysics, Chinese Academy of Sciences, Beijing, China,* [2]*University of Chinese Academy of Sciences, Beijing, China,* [3]*Key Laboratory of Petroleum Resources, Gansu Province/Northwest Institute of Eco-Environment and Resources, Chinese Academy of Sciences, Lanzhou, China*

OPEN ACCESS

Edited by:
Zhang Chengjun,
Lanzhou University, China

Reviewed by:
Yibo Yang,
Institute of Tibetan Plateau Research (CAS), China
Amzad Hussain Laskar,
Physical Research Laboratory, India
Huanye Wang,
Institute of Earth Environment (CAS), China

***Correspondence:**
Yongli Wang
wyll6800@lzb.ac.cn
Gen Wang
gwang@lzb.ac.cn

Specialty section:
This article was submitted to Quaternary Science, Geomorphology and Paleoenvironment, a section of the journal Frontiers in Earth Science

Received: *05 January 2022*
Accepted: *28 February 2022*
Published: *06 April 2022*

Citation:
Wei J, Wang Y, Wang G, Wei Z, He W, Zhang T, Ma X, Zhang P, Ma H, Yu X, Li S and Li L (2022) Biomarker Records From Eocene Lacustrine Sequence in the Eastern Tibet Plateau and Its Implication for Organic Matter Sources. Front. Earth Sci. 10:849041. doi: 10.3389/feart.2022.849041

The Eocene is the initial stage of the Cenozoic global cooling. Compared with the abundant marine records, the continental records of Eocene are scarce. Throughout the Eocene, a series of continuous deposition of gypsum and volcanic tuff-bearing red clastic sediments have developed in the Nangqian Basin (NB). In this work, representative sediments were collected from the NB, and lipid biomarkers and compound-specific carbon isotopes of *n*-alkanes were analyzed. Based on the robust paleomagnetic age–depth model, from the early to the late Eocene, the compound-specific carbon isotopic compositions ($\delta^{13}C_{23}$ and $\delta^{13}C_{25}$) increased with the sedimentary facies changed. At the same time, the relative proportion of mid-chain length to the long-chain length homologs (Paq) decreased, and the peak carbon number (C_{max}) shifted from nC_{21}, nC_{22} or nC_{23} to nC_{16}, nC_{25}, nC_{27}, or nC_{31}. We ascribed these variations to the climate drying and water level turning high as indicated by the lithology change from fluvial to lacustrine facies and the terrestrial inputs from neighboring mountain belts in the middle–late Eocene. Moreover, we compared our *n*-alkane results with other records from the TP and the global sea level and marine benthic $\delta^{18}O$. We found that a nearly synchronous deformation and drying of the eastern TP caused by the India–Asia collision in the early Eocene was closely related to the arid conditions and topographically changed in the northern TP. The climate variations in the Eocene in the NB were mainly controlled by the global climate change and the uplift of the TP and affected by the Paratethys Sea on a long scale.

Keywords: Nangqian Basin, Eastern Tibet Plateau, organic geochemistry, Eocene, lacustrine sediments

INTRODUCTION

The Eocene, which is the initial stage of the Cenozoic global climate from a "greenhouse" state to an Oligocene "icehouse" state, is considered as a "doubthouse" of global climate conditions (Zachos et al., 2008; Westerhold et al., 2020). Most of the continuous long-scale records for the Eocene paleoclimate are from ocean boreholes (Ogg and Bardot, 2001; Florindo and Roberts, 2005; Suganuma and Ogg, 2006; Edgar et al., 2010) and marine outcrops (Dallanave et al., 2009; Hollis et al., 2013; Agnini et al., 2016). In comparison with various marine records, the climate change from the evidence of lacustrine records during the Eocene, especially in the Tibetan Plateau

(TP), is little known. Recently, various geochemical records from the TP have been reported. In the northeastern TP, the Eocene strata and related paleoclimate of the Xining (Dai et al., 2006; Fang et al., 2019), Linxia (Feng et al., 2021; Feng et al., 2022), and Qaidam basins (Fang et al., 2019; Wu et al., 2021) have been reported. Based on these paleoenvironmental records, several mechanisms were formulated to interpret the environmental changes (Bosboom et al., 2011; Bosboom et al., 2014; Ding et al., 2014; Kaya et al., 2018; Westerhold et al., 2020). Furthermore, the Cenozoic sedimentary basins, especially the basin in the eastern Qiangtang Terrane, can provide an excellent record of the early India–Asia collision history during the Paleogene (Tang et al., 2017; Li et al., 2019; Li et al., 2020a; Xiong et al., 2020).

The Nangqian Basin (NB) (~32–33°N, ~96°E), in the eastern TP currently, contains a long and continuous sequence of the Eocene sediments (Horton et al., 2002; Li et al., 2019; Zhang et al., 2020). Most importantly, the NB is the intersection of the East Asian Monsoon (EAM), the Indian Monsoon (IM), and the westerlies but also the junction of the humid monsoon region in Eastern China, the arid inland region in Northwest China, and the alpine region of the TP, which is very sensitive to the changes of the environment and climate (Horton et al., 2002; Li et al., 2019). The early Cenozoic successions of gypsum and volcanic tuff-bearing red clastic sediments in the NB provide precious climatic and environmental archives (QBGMR, 1991; Horton et al., 2002; Zhang et al., 2020). Many works on the Cenozoic paleoenvironment and paleoclimate of the TP have been carried out in the NB, including the lithofacies, evaporate minerals, magnetostratigraphy, pollen-spores, clay minerals, major and trace elements, clumped isotope, carbonate oxygen, and carbon isotopes, which suggest that, with the rising altitude, the climate gradually became arid and cold in the eastern TP during the Eocene (Du et al., 2017; Yuan et al., 2017; Li et al., 2019; Fang et al., 2020; Yuan et al., 2020a; Zhang et al., 2020; Zhao et al., 2020). However, due to the lack of long sedimentary sequence and robust age constraints, the driving mechanism of the climate change is not clear.

In addition to the proxies mentioned before, lipid biomarkers originate from organisms directly, which can respond to the environment rapidly, and can be preserved in sediments stably, indicating that they preserved reliable climate records (Moldowan et al., 2005; Peters et al., 2007; Liu et al., 2015; He et al., 2020, Wang et al., 2021a, Wang et al., 2021b). *n*-Alkanes have high abundance in organisms, which can be preserved in lacustrine sediments for millions of years, and their original isotopic signals can also be well preserved (Chikaraishi and Naraoka, 2003; Aichner et al., 2010; Castañeda and Schouten, 2011; Sachse et al., 2012; Ouyang et al., 2015). For example, Liu et al. (2018) used Paq, ACL, and δD to determine the source of sedimentary *n*-alkanes and study the degree of water mass restriction (open or closed) of an ancient lake basin. Rao et al. (2016) demonstrated a complex relationship between the isotopic composition of precipitation and the precipitation amount or East Asian summer monsoon intensity by applying the compound-specific carbon and hydrogen isotopes of terrestrial long-chain *n*-alkanes. Lin et al. (2020) applied detrital zircon U–Pb geochronology and leaf wax *n*-alkane δD to analyze the surface uplift history of the Hoh Xil Basin. The *n*-alkanes and the corresponding compound-specific isotopic compositions display the application of reconstructing the paleoclimate and paleotopography in lacustrine sediments in the TP.

In the present study, the age–depth framework of the NB has been constrained by high-resolution palaeogeomagnetic records with absolute ages (Horton et al., 2002; Spurlin et al., 2005; Zhang et al., 2020). We applied the lipid biomarker (*n*-alkanes) and the corresponding compound-specific carbon isotopic compositions to reflect the variations of organic matter sources and their corresponding paleoclimate conditions. Moreover, we compared our results with other records from the TP during the Eocene to discuss the possible driving mechanisms from the perspective of biological variations.

GEOGRAPHIC AND STRATIGRAPHIC SETTING

Geological Setting

The current NB, located on the border between the Qinghai Province and the Tibet Autonomous Region, is about 4,500–5,000 m (**Figure 1A**). The India–Asia collision formed north-eastward extrusion, which facilitated a series of contraction deformation and strike-slip faults in the eastern Tibet, including the Yushu–Nangqian thrust belt and the Jinshajiang strike-slip fault system (Hou et al., 2003; Yin and Harrison, 2003; Spurlin et al., 2005). The NB is one of the series of narrow, elongated Paleogene basins in the Yushu–Nangqian region between the Songpan–Ganzi and Qiangtang terranes (**Figures 1B,C**). It is ~80 km long in the south–north direction and ~15 km wide in the east–west direction (QBGMR, 1991; Horton et al., 2002; Yuan et al., 2020).

The NB is characterized by a continental seasonal monsoon climate today and impacted by the Asian Monsoon (mainly the Indian Monsoon) (Li et al., 2019). The average annual temperature is 4.1°C, and the average annual precipitation is 538.1 mm, based on the observation from the nearest meteorological station from 1961 to 2013 (Hou et al., 2003; Wang et al., 2012; Wei and Han, 2015). The modern soils of the surrounding mountains and the basin surface are dark brown soils and steppe soils, respectively (CAS-TPET, 1985; Xiong and Li, 1990).

The Paleogene strata in the NB are characterized by prominent red beds, which contain limestone/marlite, gypsum, volcanic rock, and tuff (Horton et al., 2002; Li et al., 2019). The Neogene—Quaternary only appears sporadically in or near Paleogene basins along the Jinshajiang suture belt and is dominated by light-colored (yellow–green–gray) fluvial-dominated sediments with coals (QBGMR, 1991; Horton et al., 2002; Yuan et al., 2020a). A clear regional unconformity exists between the Paleogene and the Neogene—Quaternary (QBGMR, 1991; Horton et al., 2002; Zhang et al., 2020).

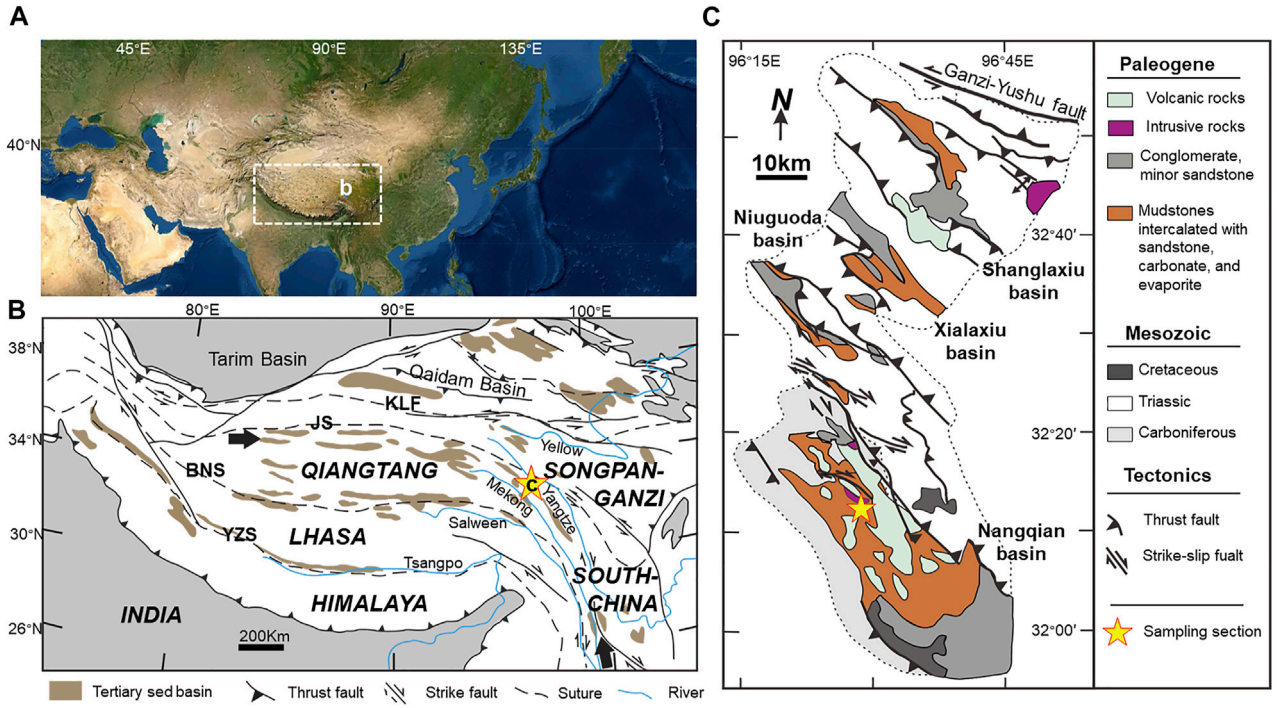

FIGURE 1 | (A) Location and **(C)** geological map of the Nangqian Basin and **(B)** neighboring basins in the eastern Tibetan Plateau. Both **(B,C)** are modified from the work of Horton et al. (2002).

Chronology

The NB contains three parts of the Paleogene deposits (QBGMR, 1991; Horton et al., 2002). Zhang et al. (2020) provided well-dated palaeogeomagnetic age of the section and the absolute age was tested using the method of zircon U–Pb dating. The lower section is dominated by brownish-red fine conglomerates, sandstones, and siltstones–mudstones, with a depth of 1,050–690 m and age of 52.5–48.0 Ma. Reddish luvic paleosols cover fine sandstone and siltstone–mudstone, with thin limestones occasionally observed (QBGMR, 1991; Horton et al., 2002; Zhang et al., 2020). A 20 m-thick andesite with an Ar–Ar age of 51.2 ± 0.2 Ma appears near the basement (Horton et al., 2002; Spurlin et al., 2005). The middle part is mainly composed of marl and limestones intercalated with reddish siltstone–mudstone, with a depth of 690–400 m and age of 48.0–43.3 Ma (Horton et al., 2002; Spurlin et al., 2005; Zhang et al., 2020). The upper part is mainly purplish-red gypsum mudstone, intercalated with a large number of thin siltstone and gypsum layers and occasionally with thin dolomite layers (QBGMR, 1991; Horton et al., 2002). The depth of the upper part is 400–0 m and the age of that is 43.3–35 Ma (Zhang et al., 2020). Volcanic tuff rocks were found in this part, with an Ar–Ar age of 38.2 ± 0.1 Ma (Horton et al., 2002; Spurlin et al., 2005) and a zircon U–Pb age of 37.3 ± 0.56 Ma (Zhang et al., 2020). The lithological change is interpreted as a gradual transition drought from a braided river, alluvial fan, and ephemeral shallow pond/lake environment to a semi-brackish lake in a distal floodplain and finally to playa mudflat and saline lake environments (**Figure 2B**).

SAMPLING AND METHODS

The Nangqian section is located along the Zhaqu River with a total thickness of 1050 m (**Figure 1**). According to lithology, a total of 67 bulk samples were selected. The 67 sediment samples were collected from 52.5 to 35 Ma in a depth interval from 0 to 1,050 m. Before collecting samples, the weathering denudation surface was knocked out with a geological hammer. Then, fresh samples were obtained and put into degreasing cloth bags for storage.

Biomarker Analyses

In this study, 22 samples were tested for biomarker analyses (**Supplementary Table S1**). The 22 samples are divided into two sections. There are 12 samples in the lower section (age 51.8–46.4 Ma) and 10 samples in the upper section (age 42.3–35.5 Ma).

The extraction process of biomarkers is as follows: the bulk samples were extensively cleaned to remove any possible contamination from recent organic material and crushed to fine powder larger than 100 mesh. Powdered samples (~400 g) were weighed into pre-extracted filter paper thimbles (the filter paper was extracted using a Soxhlet extractor with DCM for 72 h previously) and Soxhlet extracted at 50°C continuously for 72 h using a Soxhlet extractor (DCM: MeOH = 9:1, v:v). The glassware used in this experiment, such as injection bottle, weighing bottle, and conical bottle, had been washed with acetone, rinsed with clean water and ultrapure water, dried in an oven, sealed with clean tinfoil, and then, burned (400°C for 5 h) in a muffle furnace

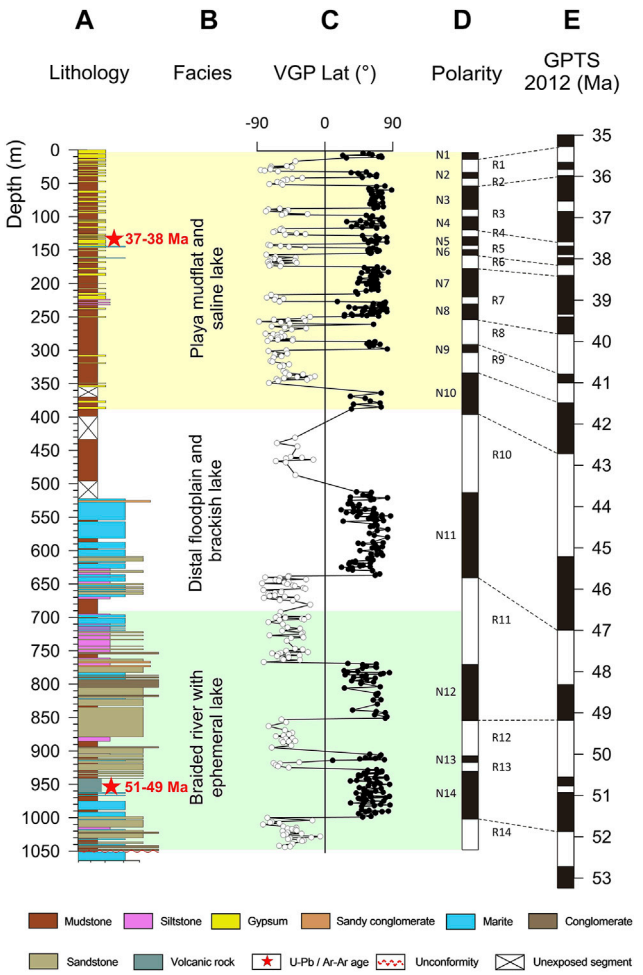

FIGURE 2 | Lithofacies **(A)** and sedimentary facies **(B)** of the Paleogene sedimentary sequence in the NB. The magnetostratigraphy **(C–E)** is modified from the work of Zhang et al. (2020). The Ar–Ar and U–Pb ages are from the work of Horton et al. (2002), Spurlin et al. (2005), and Zhang et al. (2020).

previously. Tweezers and other tools were washed with DCM 2–3 times before used.

Total lipid extracts were loaded onto a solid phase extraction column (ANPEL, silica gel 500 mg). The *n*-alkanes were eluted with *n*-hexane (5–10 ml). After drying *n*-alkanes, 1 μL of the sample in hexane was injected into a GC–MS-QP2020NX (Shimadzus, Japan). This instrument was equipped with an Rtx-5 MS gas chromatograph which was fitted with a 30 m × 0.25 mm i. d. fused silica capillary column, coated with a film (0.25 μm) of 5% phenyl-methyl-DB-5. The carrier gas was 99.995% high purity helium, and the control mode was linear velocity. The heating program was set as follows: initially at 80°C for 2 min, rapidly increased to 210°C at a rate of 4°C/min, then increased from 210 to 295°C at a rate of 3°C/min, and held at 295°C for 20 min. The column flow rate was 1.0 ml/min, and the injection volume was 1 μL. The diversion mode showed no diversion. The MS was operated with ionization energy of 70 eV, and the temperature of ion source was 250°C. The GC–MS was tuned using perfluorotributylamine (PFTBA) and blank samples were analyzed to check the background. The interface temperature of GC–MS was 300°C. The solvent delay was set to 2 min. Both GC–MS scan and GC–MS single ion monitoring mode (SIM) were used for acquisition.

Compound-Specific $\delta^{13}C$ Analyses

According to the preliminary results of 22 biomarkers, 23 samples were selected for the test of compound-specific carbon isotopic compositions (**Supplementary Table S1**). There were 12 samples in the lower section and 11 samples in the upper section. The extraction process of *n*-alkanes for compound-specific carbon isotopic compositions was the same as that described in *Biomarker Analyses*.

The test of carbon isotopic values of individual *n*-alkanes was finished on a GC (Agilent 6,890) coupled to an isotope ratio mass spectrometer (IRMS, Thermo Scientific MAT 253) via a combustion interface (GC Combustion III) (Key Laboratory of Petroleum Resources Research, Chinese Academy of Sciences). High-purity helium was used as a carrier gas at 2 ml min^{-1}. The gas chromatograph was fitted with a 30 m × 0.32 mm i. d. fused silica capillary column, coated with a film (0.25 μm). The oven temperature was programmed to be initially held at 80°C for 3 min, increased to 300°C at a rate of 3°C/min, and held for another 30 min. Individual compounds were oxidized at 940°C when flowing through an oxidation ceramic micro-reactor filled with twisted wires (NiO/CuO/Pt). Three pulses of standard pure CO_2 gas, pre-calibrated against a commercial reference CO_2, were injected via the GC-C III interface to the IRMS for the computation of $\delta^{13}C$ values of sample compounds. A set of *n*-alkanes (*n*-alkane mixture type A7) with known $\delta^{13}C$ values acquired from Indiana University were measured daily to ensure the accuracy of the machine. The standard deviation for duplicate analyses of this standard was <± 0.3‰. The $\delta^{13}C$ values were reported with reference to the PDB standard. The resolution of hydrocarbon peaks obtained during GC–IRMS was similar to that obtained in GC–MS analysis.

Calculation of Biomarker Proxies

As for the biomarker proxies, the index of proportion of aquatic plants (Paq, Ficken et al., 2000) values was calculated as follows:

$$Paq = (nC_{23} + nC_{25})/(nC_{23} + nC_{25} + nC_{29} + nC_{31}).$$

The carbon preference index (CPI) values of the extracted long-chain *n*-alkanes (nC_{26} to nC_{34}) were calculated using a modified formula of Cranwell (1984) and Ratnayake et al. (2006) as follows:

$$CPI = 1/2\left[\frac{(nC_{27} + nC_{29} + nC_{31} + nC_{33})}{(nC_{26} + nC_{28} + nC_{30} + nC_{32})} + \frac{(nC_{27} + nC_{29} + nC_{31} + nC_{33})}{(nC_{28} + nC_{30} + nC_{32} + nC_{34})}\right].$$

The average chain length (ACL) values were calculated using a modified formula of Poynter et al. (1989) as follows:

$$ACL_{27-33} = (27 \times nC_{27} + 29 \times nC_{29} + 31 \times nC_{31} + 33 \times nC_{33})/ \times (nC_{27} + nC_{29} + nC_{31} + nC_{33}).$$

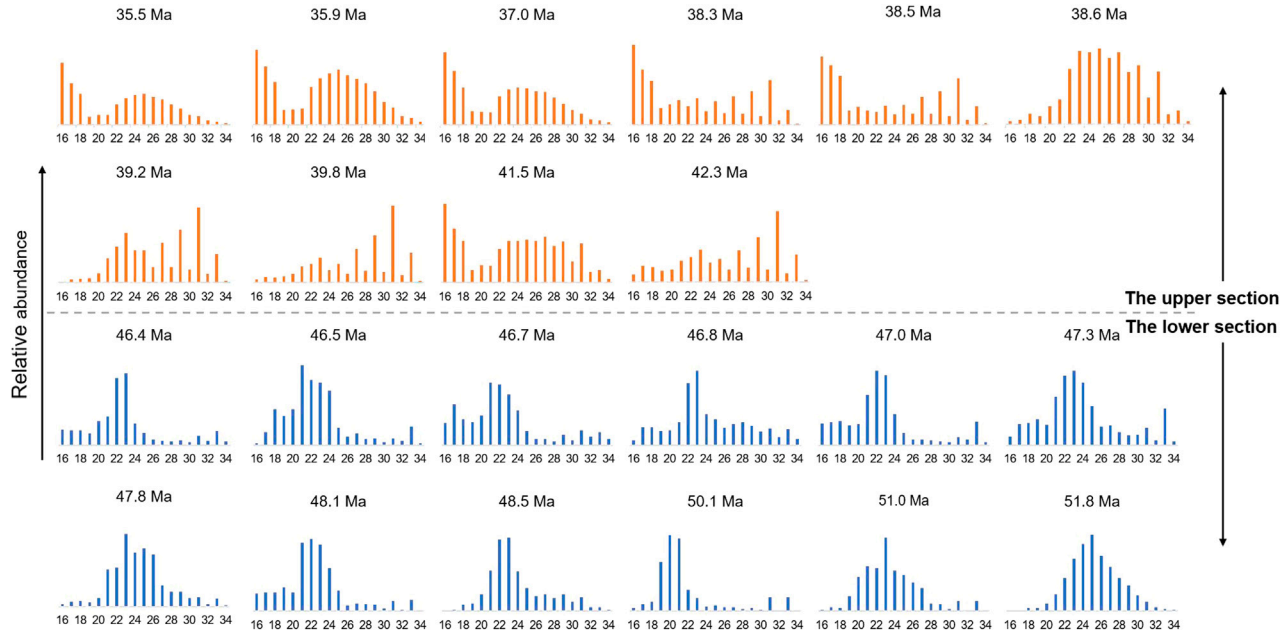

FIGURE 3 | Distribution patterns of *n*-alkanes in the NB.

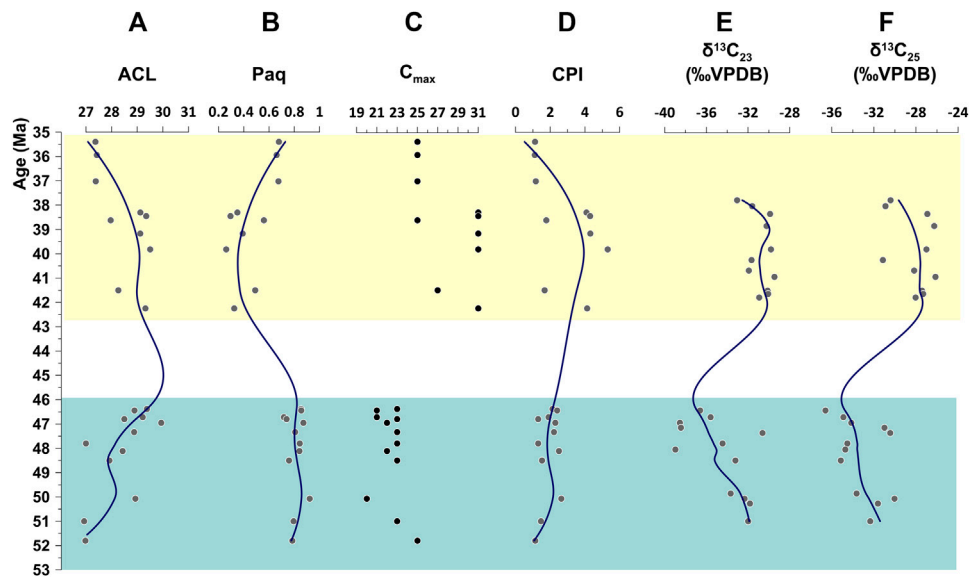

FIGURE 4 | Climate and environmental proxy records of ACL **(A)**, Paq **(B)**, C_{max} **(C)**, CPI **(D)** proxies, and compound-specific carbon isotopic compositions of nC_{23} and nC_{25} **(E,F)** in the NB. LOESS Fit (0.5 span for a, b, and d, 0.4 span for e and 0.55 span for **(F)**. The green and yellow shaded areas mark the lower section and the upper section.

RESULTS

The distribution patterns of *n*-alkanes in the NB sediments are shown in **Figure 3**. The distribution of *n*-alkanes in the 12 samples of the lower section is mainly unimodal and maximized at nC_{21}, nC_{22}, or nC_{23}. The distribution of *n*-alkanes in the other 10 samples of the upper section is mainly bimodal and mainly maximized at nC_{16}, nC_{25}, nC_{27}, or nC_{31}.

The Paq and CPI values of the two sections changed significantly (**Figures 4B,D**). In the lower section, the Paq values were between 0.72 and 0.92, with an average of 0.82. In

the upper section, the Paq values were between 0.26 and 0.68, and the average value was 0.47. Meanwhile, the average value of CPI increased from the lower section to the upper section, with an average of 1.90 to an average of 2.90.

In **Figures 4E,F**, compound-specific carbon isotopic compositions ($\delta^{13}C_{23}$ and $\delta^{13}C_{25}$) were heavier in the upper section than those in the lower section. From the lower to the upper section, the average of $\delta^{13}C_{23}$ changed from −34.69‰ to −30.79‰, and $\delta^{13}C_{25}$ showed a similar increase from an average of −33.26‰ to an average of −28.16‰.

DISCUSSION

Degradation Degree of *n*-Alkanes in the Nangqian Basin

For *n*-alkanes, their typical odd-to-even preference in the long-chain part suggests a low degree of degradation (Luo et al., 2012; Duan et al., 2020). In sediments, CPI >1 means a predominance of odd over even chain lengths (Eglinton and Hamilton, 1967). Sediments from the upper section of the NB are characterized with CPI >1, except for the top three samples (age of 35.5, 35.9, and 37.0 Ma), indicating a low degree of degradation. In the lower section, although the CPI >1 was not remarkable, the odd-to-even preference is still observed in the low proportion of the long-chain *n*-alkanes (according to the distribution patterns in **Figure 3**). Combined with the analysis of organic sources reflected by the distribution patterns of *n*-alkanes, the low CPI values in the lower section was the result of the small input of terrestrial plants, which made the odd-to-even preference in the long-chain *n*-alkanes difficult to observe. Therefore, it can be concluded that the degradation of *n*-alkanes in this study would not affect the restoration of paleoenvironment.

Variations in Biomarker Proxies and δ^{13}Calk

Previous studies have shown that the mid-chain length *n*-alkanes are mainly from aquatic plants, such as submerged and floating plants (Meyers and Ishiwatari, 1993; Ficken et al., 2000; Yu et al., 2021). However, the contribution of terrestrial plants to the mid-chain *n*-alkanes is inevitable, especially in the upper section (**Figure 3**). Nevertheless, the carbon source of terrestrial plants is atmospheric CO_2 and that of aquatic organisms is HCO_3^- (Meyers and Ishiwatari, 1993; Meyers, 2003; Wang et al., 2013), possibly resulting in the different composition of $\delta^{13}C$ values. The $\delta^{13}C$ value of HCO_3^- is heavier than that of atmospheric CO_2, leading to more negative $\delta^{13}C$ values of terrestrial plants, indicating that if the $\delta^{13}C$ value of mid-chain *n*-alkanes (nC_{23} and nC_{25}) was seriously influenced by terrestrial plants, more negative $\delta^{13}C$ values were likely to be observed in the upper section. However, the $\delta^{13}C$ value of mid-chain *n*-alkanes (nC_{23} and nC_{25}) increased in the upper section, displaying an opposite trend, which indicates that the influence of terrestrial plants on the compound-specific carbon isotopic compositions of the mid-chain *n*-alkanes was limited. Therefore, in this study, we proposed that the nC_{23} and nC_{25} were contributed by the aquatic plants.

Jiang et al. (2021) investigated the $\delta^{13}C_{org}$ values of surface sediment samples from 55 lakes in the mid-latitude Asia to establish the relationship between the $\delta^{13}C$ value of aquatic organisms and water depth in lacustrine settings. In freshwater and brackish lakes, $\delta^{13}C_{org}$ variation resembles an arched pattern with depth, with relatively positive $\delta^{13}C_{org}$ values corresponding to the depth of ~1–10 m. According to the sedimentary facies in the NB (**Figure 2B**), it transited from the braided river, alluvial fan, and ephemeral shallow pond/lake environment to a semi-brackish lake in a distal floodplain predominates, suggesting that the lake level in the NB in the mid–late Eocene was higher than that in the early Eocene. The lake water level recorded by $\delta^{13}C_{23}$ and $\delta^{13}C_{25}$ is consistent with the variations of sedimentary facies (**Figures 4E,F**), showing a relative higher water level in the mid–late Eocene.

In addition, *n*-alkanes can truly reflect the input characteristics of parent material sources (Meyers, 2003). Ficken et al. (2000) proposed the Paq index to indicate the non-emergent (submerged and floating-leaved) aquatic plants input to lake sediments relative to that from the emergent aquatic and terrestrial plants, which expresses the relative proportion of mid-chain length (nC_{23}, nC_{25}) *n*-alkanes to long-chain length (nC_{29}, nC_{31}) homologs. Further studies have indicated that the Paq value can be used to represent the effective moisture and water level, and basically, the larger the Paq, the more hydrocarbon input from aquatic organisms, the more precipitation and the wetter climate (Nichols et al., 2006; Pu et al., 2011; Zheng et al., 2007). In the Linggo Lake, the high Paq with the heavy δD_{alk} implied abundant precipitation brought by the westerlies, indicating that the Linggo Lake was at a high water level under a humid environment (Hou et al., 2003). In the present study, the average value of Paq decreased from 0.82 (ranging from 0.72 to 0.92) to 0.47 (ranging from 0.26 to 0.68) (**Figure 4B**). The decrease of Paq in the NB is contrary to the high water level as recorded by sedimentary facies and compound-specific carbon isotopic compositions, which implied that the Paq values were affected by other factors (Liu et al., 2015).

Judging from the provenance analysis of sediments in the NB (Zhang et al., 2019), the initially accumulated sediments of the NB has changed from relatively small internal drainage networks and short main-stem rivers in this region in the Paleocene to the nearby thrust belts in the Eocene (Horton et al., 2002; Spurlin et al., 2005). Based on the stable and clumped isotopic evidence of carbonates, the NB was 2.7 (+0.6/−0.4) km in elevation while the hypsometric mean elevation of surrounding mountains was 3.0 ± 1.1 km above sea level during the late Eocene (Li et al., 2020b). In addition, palynology records indicated that the high-elevation genus *Tsugaepollenites* presented in the Ria Zhong section in the NB in the late Eocene (Yuan et al., 2020a; Yuan et al., 2020b). In addition, the crustal deformation and thickening induced by intracontinental subduction between the Lhasa and Qiangtang terranes caused a rapid uplift of the Central Watershed Mountain, associated with the regional climate change transforming the landscape from desert to forest in the Gonjo Basin (Xiong et al., 2020). In view of the previous studies, the specific tectonic settings can further explain this topographic difference in the NB. Spurlin et al. (2005) proposed that a nearly 40% upper-crustal shortening, occurring in the early Cenozoic, was observed over the area,

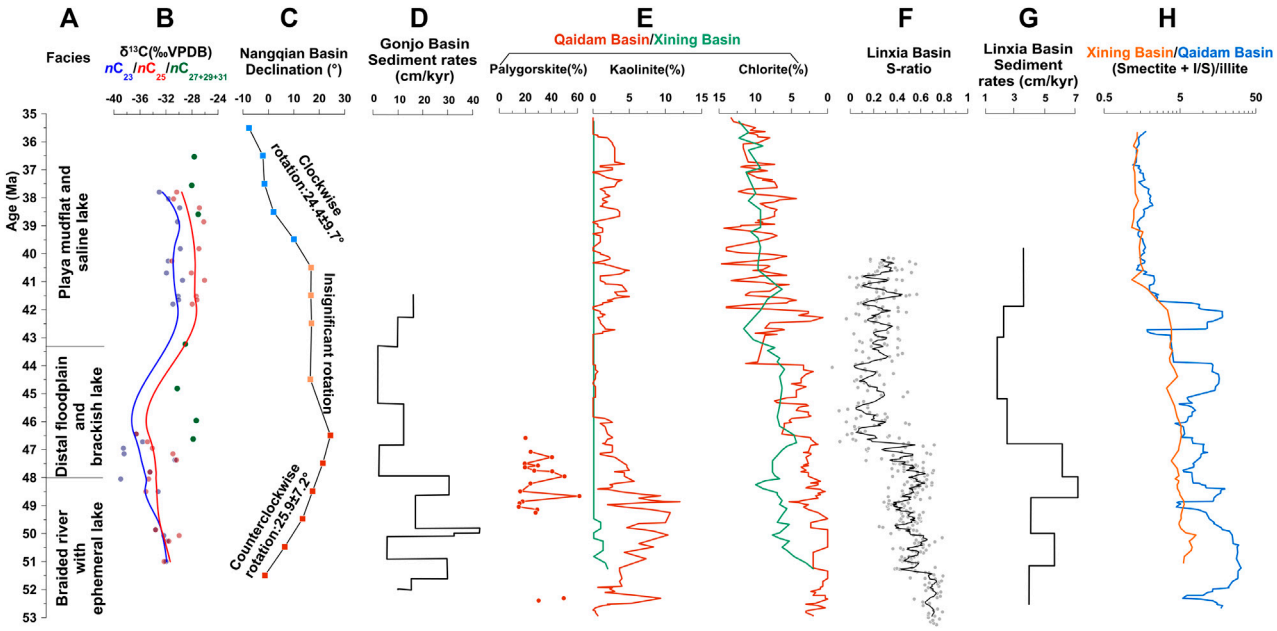

FIGURE 5 | Summarized paleoclimatic records of the Eocene in the Tibetan Plateau. **(A)** sedimentary facies in the Nangqian Basin (this study); **(B)** red and blue dots and corresponding fitted curve (0.4 span for nC_{23} and 0.55 span for nC_{25}) indicating the $\delta^{13}C$ of mid-chain alkanes nC_{23} and nC_{25} from the Nangqian Basin (this study), and the $\delta^{13}C$ values averaged over the three long-chain alkanes nC_{27}, nC_{29} and nC_{31} from the Qaidam Basin (Sun et al., 2020); **(C)** Tectonic rotational history of the northeastern central TP, based on mean declination of every 1 Ma stratigraphic interval of the NB (Zhang et al., 2020); **(D)** the sediment accumulation rates of the Gonjo Basin (Li et al., 2020); **(E)** Clay mineral assemblages in the Qaidam Basin and Xining Basin, respectively (Ye et al., 2018; Fang et al., 2019) (3-point running averages for kaolinite and chlorite); **(F)** S-ratio for the DHJ section in the Linxia Basin (Feng et al., 2021); **(G)** the sediment accumulation rates of the Linxia Basin (Feng et al., 2022); **(H)** (Smectite + I/S)/illite ratios in the Hongliugou and Xiejia sections in the Qaidam and Xining Basins, respectively (Fang et al., 2019).

which accounted for most of the surface uplift of the Nangqian region. Horton et al. (2002) proposed that the fold-thrust belts were the consequence of contraction triggered by the India–Asia collision. Based on the previous studies, in the mid—late Eocene, the Nangqian region appeared as small intermontane sub-basins and received plentiful terrestrial sediments from the neighboring mountain belts. The Paq, ACL, and C_{max} contain the common information of terrestrial plants from nearby mountains and aquatic plants from the playa lake/mudflat, so the water level was no longer the sole factor affecting Paq. This explained why Paq values showed the opposite result of sedimentary facies when interpreting the water level.

Evaporite minerals are also sensitive to environmental and climatic changes (Warren, 2000, 2006; Meister et al., 2011; Zhu et al., 2021; Zhang et al., 2021; Zhang et al., 2022). In the mid—late Eocene, gypsum, a typical evaporite mineral, indicated a dry climate in the NB, which was absent in the early Eocene (Yuan et al., 2020b; Zhang et al., 2020). The adjacent areas, such as the Gonjo Basin, Qaidam Basin, and Tarim Basin, showed a succession of gypsiferous red beds with an upward increase in evaporites (Wang et al., 2008; Wang et al., 2016; Tang et al., 2017; Li et al., 2020a; Xiong et al., 2020), further suggesting an increasingly arid climate.

To sum up, the climate in the early and mid—late Eocene was completely different. In the early Eocene, the terrain was generally low and flat, with a humid climate and low water level. After the tectonic movements caused by the India–Asia collision, the NB and surrounding areas appeared as small intermontane sub-basins, characterized by an arid climate.

Driving Mechanisms of Eocene Climate Variations in the Eastern Tibetan Plateau

From the early to the late Eocene, the sedimentary facies and the water level recorded by compound-specific $\delta^{13}C$ in the present study implied a notable climate transition from humid to arid conditions and a topographical change in the eastern TP.

Previous studies have indicated that three main forcing mechanisms, including the uplift of the Tibetan Plateau, the retreat or incursion of the Paratethys Sea, and global cooling, may be responsible for the change (Bosboom et al., 2011; Bosboom et al., 2014; Ding et al., 2014; Kaya et al., 2018; Westerhold et al., 2020).

The global cooling could be a first-order control in the NB beyond the impact of the India–Asia collision and the retreat or incursion of the Paratethys Sea. The global cooling reduced evaporation from the sea and thus the water vapor flux to the air (Fang et al., 2019; Westerhold et al., 2020). The rapid global sea level fall accompanied by the shrinking of the sea area increased the distance from the study area to the sea, which reduced the marine-derived water vapor supply (Miller et al., 2020). Via the modulation of the water vapor supply by the westerlies, the long-term global cooling in the Eocene reduced the water vapor supply to the continental and, thus, caused further

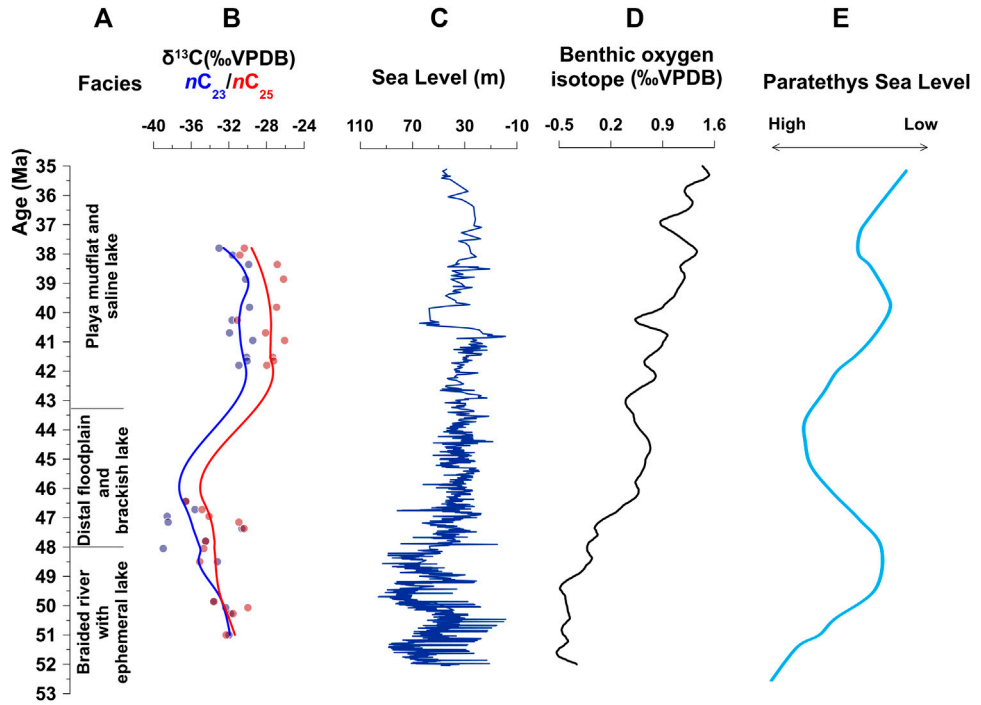

FIGURE 6 | (A) Sedimentary facies in the Nangqian Basin (this study); **(B)** red and blue dots and the corresponding fitted curve indicating the $\delta^{13}C$ of mid-chain alkanes nC_{23} and nC_{25} from the Nangqian Basin (this study); **(C)** global sea level curve (Miller et al., 2020); **(D)** marine benthic oxygen isotopic compositions (Westerhold et al., 2020); **(E)** sea level of the Paratethys Sea (Bosboom et al., 2014).

drying in the NB. Furthermore, the good correlation between the water level and climate in the NB, the northeastern TP, and the global climate proxies implied that the global climate system served as the main driver of climate variations in the study area (Westerhold et al., 2020; **Figure 5H**, **Figure 6A–D**).

Exploring the past topography is essential for disentangling the complex interactions between orography and climate (Fang et al., 2019; Xiong at el., 2020; Wu et al., 2021). Our records reflected a significant early Eocene deformation and climate change in response to the India–Asia collision. From the paleomagnetic evidence, a counterclockwise rotation of 25.9 ± 7.2° during 52–46 Ma supported the basin deposition, rotation, and volcanism by northward compression and eastward extrusion of the eastern Lhasa and Qiangtang Blocks as early response to the India–Asia collision (**Figure 5C**). During ~52–48 Ma, a relatively high sedimentation rate in the Gonjo Basin suggested an active tectonic setting in the eastern TP, which coincided with the clockwise rotation (**Figure 5D**, Li et al., 2020b). Interestingly, a relatively low sedimentation rate appeared in the Gonjo Basin at ~48–41 Ma, which coexisted with a rapid sedimentation rate decrease in the Linxia Basin at ~47–40 Ma (**Figure 5G**). The paleomagnetic results in the Xining Basin revealed a stable tectonic setting with no significant rotation at ~48–41 Ma (Dupont-Nivet et al., 2008). In addition, an arid environment appeared at ~49.5–47 Ma in the Qaidam Basin and Xining Basin recorded by palygorskite, kaolinite, and chlorite (**Figure 5E**, Ye et al., 2018; Fang et al., 2019) and at 47.6 Ma in the Linxia Basin recorded by the S-ratio (**Figure 5F**, Feng et al., 2021), which coincided with arid climate conditions recorded by transitions of sedimentary facies in the NB (**Figure 5A**), suggesting a nearly synchronous deformation and climate change across the eastern and northern Tibetan Plateau in the early Eocene. These analyses show that the India–Asia collision could be the most direct factor of climate change in the NB, and the eastern TP.

A vast shallow epicontinental sea extended across Eurasia and was well-connected to the Western Tethys before it retreated westward and became isolated as the Paratethys Sea during the Paleogene (Bosboom et al., 2014). It regulated the hydrological cycle in Central Asia by the westerlies, so the westward retreat of this sea was as important as the Tibetan Plateau uplift in forcing aridification in the Asian continental interior (Dupont-Nivet et al., 2007). Previous studies on the Tarim and Tajik basins indicate that there were three sea-level cycles during 52–35 Ma (**Figure 6E**) (Bosboom et al., 2014; Kaya et al., 2018). However, due to the lack of data in our section between 46 and 43 Ma, it is difficult to assess the impact of Paratethys Sea on the aridity of the eastern TP. For all that, the influence of Paratethys Sea would be long-term and gradual, and the stepwise sea retreat from Central Asia amplified the aridification of the Asian interior (Bosboom et al., 2014; Carrapa et al., 2015; Sun et al., 2016; Kaya et al., 2018). From **Figure 2A**, the trend of gradual drought in the NB has been well recorded by the lithology change. Although the retreat or incursion of the Paratethys Sea failed to compare with the organic records in NB, it is still an important factor worthy of further research.

In general, our observations recorded a significant change in sedimentary facies from braided river facies to brackish lake facies in the early-mid Eocene in the eastern TP. At the same time, the compound-specific carbon isotopic compositions of *n*-alkane ($\delta^{13}C_{23}$ and $\delta^{13}C_{25}$) recorded the rise of the lake level. In the mid–late Eocene in the NB, the terrestrial input in the sediments increased, which corresponded to the climate drying and topographic change at this time. In comparison with three main driving mechanisms, our records were consistent with global climate changes, related closely with the India–Asia collision in the early Eocene, and the relevance with Paratethys Sea needs further study. We claim that the climate variations in the Eocene in the study area were mainly controlled by the global climate change and the uplift of the Tibetan Plateau, but the impact of the Tethys Sea cannot be ignored.

CONCLUSION

We applied the *n*-alkanes and the compound-specific carbon isotopic compositions in the NB to reflect the paleoclimate conditions in the eastern Tibet Plateau. From our multi-proxy records, we came to the conclusion that the NB underwent rapid drying from the early to the mid–late Eocene. The compound-specific carbon isotopic compositions ($\delta^{13}C_{23}$ and $\delta^{13}C_{25}$) were affected by the water level deepening and showed a rapid positive. From the *n*-alkene records in the NB, the type of aquatic organism in the Eocene lacustrine sequence had an evident change from submerged and floating plants to emergent and terrestrial plants, responding to climate drying and orographic uplifting. Meanwhile, the lithofacies changed from the braided river, alluvial fan, and ephemeral shallow pond/lake environment to a semi-brackish lake in a distal floodplain and finally to playa mudflat and saline lake environments. We regard the change of multi-proxy records by *n*-alkenes consistent with the sedimentary facies change and aridity in the NB and responded synchronously in the northern TP, which was mainly controlled by the global cooling and the uplift of the Tibetan Plateau and affected by the Paratethys Sea on a long scale.

DATA AVAILABILITY STATEMENT

The original contributions presented in the study are included in the **Supplementary Material**, further inquiries can be directed to the corresponding authors.

AUTHOR CONTRIBUTIONS

JW: participation in the whole work and drafting of the article; YW, GW, and ZW: perception and design and final approval of the version to be published; and WH, TZ, XM, PZ, HM, XY, SL, and LL: data analysis.

FUNDING

This work was supported by the National Natural Science Foundation of China (grant numbers 41831176), the Second Tibetan Plateau Scientifc Expedition and Research (STEP) Program (grant number 2019QZKK0707), the Strategic Priority Research Program of CAS (grant numbers XDB26000000), the National Natural Science Foundation of China (grant numbers 41902028, 41972030, 42072038 and 41888101), the National Key R and D Program of China (grant number 2017YFA0604803), the CAS "Light of West China" Program and the Youth Innovation Promotion Association CAS (No. 2021425).

SUPPLEMENTARY MATERIAL

The Supplementary Material for this article can be found online at: https://www.frontiersin.org/articles/10.3389/feart.2022.849041/full#supplementary-material

REFERENCES

Agnini, C., Spofforth, D. J. A., Dickens, G. R., Rio, D., Pälike, H., Backman, J., et al. (2016). Stable Isotope and Calcareous Nannofossil Assemblage Record of the Late Paleocene and Early Eocene (Cicogna Section). *Clim. Past* 12, 883–909. doi:10.5194/cp-12-883-2016

Aichner, B., Herzschuh, U., and Wilkes, H. (2010). Influence of Aquatic Macrophytes on the Stable Carbon Isotopic Signatures of Sedimentary Organic Matter in Lakes on the Tibetan Plateau. *Org. Geochem.* 41, 706–718. doi:10.1016/j.orggeochem.2010.02.002

Bosboom, R., Dupont-Nivet, G., Grothe, A., Brinkhuis, H., Villa, G., Mandic, O., et al. (2014). Timing, Cause and Impact of the Late Eocene Stepwise Sea Retreat from the Tarim Basin (West China). *Palaeogeogr. Palaeoclimatol. Palaeoecol.* 403, 101–118. doi:10.1016/j.palaeo.2014.03.035

Bosboom, R. E., Dupont-Nivet, G., Houben, A. J. P., Brinkhuis, H., Villa, G., Mandic, O., et al. (2011). Late Eocene Sea Retreat from the Tarim Basin (West China) and Concomitant Asian Paleoenvironmental Change. *Palaeogeogr. Palaeoclimatol. Palaeoecol.* 299, 385–398. doi:10.1016/j.palaeo.2010.11.019

Carrapa, B., DeCelles, P. G., Wang, X., Clementz, M. T., Mancin, N., Stoica, M., et al. (2015). Tectono-climatic Implications of Eocene Paratethys Regression in the Tajik basin of central Asia. *Earth Planet. Sci. Lett.* 424, 168–178. doi:10.1016/j.epsl.2015.05.034

CAS-TPET (CAS Plateau Expedition Team) (1985). *Soil of Xizang (Tibet)*. Beijing: Science Press, 1–313. (in Chinese with English abstract).

Castañeda, I. S., and Schouten, S. (2011). A Review of Molecular Organic Proxies for Examining Modern and Ancient Lacustrine Environments. *Quat. Sci. Rev.* 30, 2851–2891. doi:10.1016/j.quascirev.2011.07.009

Chikaraishi, Y., and Naraoka, H. (2003). Compound-specific δD-δ13C Analyses of N-Alkanes Extracted from Terrestrial and Aquatic Plants. *Phytochemistry* 63, 361–371. doi:10.1016/s0031-9422(02)00749-5

Cranwell, P. A. (1984). Lipid Geochemistry of Sediments from Upton Broad, a Small Productive lake. *Org. Geochem.* 7, 25–37. doi:10.1016/0146-6380(84)90134-7

Dai, S., Fang, X., Dupont-Nivet, G., Song, C., Gao, J., Krijgsman, W., et al. (2006). Magnetostratigraphy of Cenozoic Sediments from the Xining Basin: Tectonic Implications for the Northeastern Tibetan Plateau. *J. Geophys. Res.* 111, a–n. doi:10.1029/2005jb004187

Dallanave, E., Agnini, C., Muttoni, G., and Rio, D. (2009). Magneto-biostratigraphy of the Cicogna Section (Italy): Implications for the Late

Paleocene-Early Eocene Time Scale. *Earth Planet. Sci. Lett.* 285, 39–51. doi:10.1016/j.epsl.2009.05.033

Ding, L., Xu, Q., Yue, Y., Wang, H., Cai, F., and Li, S. (2014). The Andean-type Gangdese Mountains: Paleoelevation Record from the Paleocene-Eocene Linzhou Basin. *Earth Planet. Sci. Lett.* 392, 250–264. doi:10.1016/j.epsl.2014.01.045

Du, H. F., Jiang, Y. Y., Jiang, Y. B., and Yan, Z. B. (2017). Characteristics of gypsum-salt and Sulfur Isotopes in the Gonjo Formation of Nangqen Paleogene basin. *J. East China Univ. Tech.* 40, 165–172. (in Chinese with English abstract). doi:10.3969/j.issn.1674-3504.2017.02.009

Duan, Y., Wu, Y., Xing, L., Li, Z., and Zhang, T. (2020). Experimental Simulation Study on the Influence of Diagenetic Water Medium on Sedimentary *N*-Alkanes and Their Respective Hydrogen Isotopes. *Fuel* 272, 117704. doi:10.1016/j.fuel.2020.117704

Dupont-Nivet, G., Hoorn, C., and Konert, M. (2008). Tibetan Uplift Prior to the Eocene-Oligocene Climate Transition: Evidence from Pollen Analysis of the Xining Basin. *Geol* 36, 987–990. doi:10.1130/g25063a.1

Dupont-Nivet, G., Krijgsman, W., Langereis, C. G., Abels, H. A., Dai, S., and Fang, X. (2007). Tibetan Plateau Aridification Linked to Global Cooling at the Eocene-Oligocene Transition. *Nature* 445, 635–638. doi:10.1038/nature05516

Edgar, K. M., Wilson, P. A., Sexton, P. F., Gibbs, S. J., Roberts, A. P., and Norris, R. D. (2010). New Biostratigraphic, Magnetostratigraphic and Isotopic Insights into the Middle Eocene Climatic Optimum in Low Latitudes. *Palaeogeogr. Palaeoclimatol. Palaeoecol.* 297, 670–682. doi:10.1016/j.palaeo.2010.09.016

Eglinton, G., and Hamilton, R. J. (1967). Leaf Epicuticular Waxes. *Science* 156, 1322–1335. doi:10.1126/science.156.3780.1322

Fang, X., Dupont-Nivet, G., Wang, C., Song, C., Meng, Q., Zhang, W., et al. (2020). Revised Chronology of central Tibet Uplift (Lunpola Basin). *Sci. Adv.* 6. doi:10.1126/sciadv.aba7298

Fang, X., Galy, A., Yang, Y., Zhang, W., Ye, C., and Song, C. (2019). Paleogene Global Cooling-Induced Temperature Feedback on Chemical Weathering, as Recorded in the Northern Tibetan Plateau. *Geology* 47, 992–996. doi:10.1130/g46422.1

Feng, Z., Zhang, W., Fang, X., Zan, J., Zhang, T., Song, C., et al. (2022). Eocene Deformation of the NE Tibetan Plateau: Indications from Magnetostratigraphic Constraints on the Oldest Sedimentary Sequence in the Linxia Basin. *Gondwana Res.* 101, 77–93. doi:10.1016/j.gr.2021.07.027

Feng, Z., Zhang, W., Zhang, T., Fang, X., Zan, J., Yan, M., et al. (2021). Early-Middle Eocene Hydroclimate Variations Recorded by Environmental Magnetism in the Linxia Basin, NE Tibetan Plateau. *Paleoceanogr Paleoclimatol* 36, e2021PA004338. doi:10.1029/2021PA004338

Ficken, K. J., Li, B., Swain, D. L., and Eglinton, G. (2000). An *N*-Alkane Proxy for the Sedimentary Input of Submerged/floating Freshwater Aquatic Macrophytes. *Org. Geochem.* 31, 745–749. doi:10.1016/S0146-6380(00)00081-4

Florindo, F., and Roberts, A. P. (2005). Eocene-Oligocene Magnetobiochronology of ODP Sites 689 and 690, Maud Rise, Weddell Sea, Antarctica. *Geol. Soc. America Bull.* 117, 46–66. doi:10.1130/b25541.1

He, W., Wang, G., Wang, Y., Wei, Z., Huang, Z., and Zhang, T. (2020). Microbial Communities and Lipid Records of the Linxia Basin, NE Tibetan Plateau: Implications for Enhanced Aridity in the Late Miocene. *J. Asian Earth Sci.* 193. doi:10.1016/j.jseaes.2020.104290

Hollis, C. J., Taylor, K. W. R., Handley, L., Pancost, R. D., Huber, M., Creech, J. B., et al. (2013). Erratum to "Early Paleogene Temperature History of the Southwest Pacific Ocean: Reconciling Proxies and Models" [Earth Planet53–66]. *Sci. Lett.Earth Planet. Sci. Lett.* 374, 258–259. doi:10.1016/j.epsl.2013.06.012

Horton, B. K., Yin, A., Spurlin, M. S., Zhou, J. Y., and Wang, J. H. (2002). Paleocene–Eocene Syncontractional Sedimentation in Narrow, Lacustrine-Dominated Basins of East-central Tibet. *Geol. Soc. Am. Bull.* 114, 771–786. doi:10.1130/0016-7606(2002)114<0771:PESSIN>2.0.CO;2

Hou, Z. Q., Ma, H. W., Zaw, K., Zhang, Y. Q., Wang, M. J., Wang, Z., et al. (2003). The Himalayan Yulong Porphyry Copper Celt: Product of Large-Scale Strike-Slip Faulting in Eastern Tibet. *Econ. Geol.* 98, 125–145. doi:10.2113/98.1.125

Jiang, J. W., Meng, B. W., Liu, H., Wang, H. Y., Kolpakova, M., Krivonogov, S., et al. (2021). Water Depth Control on *N*-Alkane Distribution and Organic Carbon Isotope in Mid-latitude Asian Lakes. *Chem. Geol.* 565, 120070. doi:10.1016/j.chemgeo.2021.120070

Kaya, M. Y., Dupont-Nivet, G., Proust, J.-N., Roperch, P., Bougeois, L., Meijer, N., et al. (2018). Paleogene Evolution and Demise of the Proto-Paratethys Sea in central Asia (Tarim and Tajik Basins): Role of Intensified Tectonic Activity at Ca. 41 Ma. *Basin. Res.* 31, 461–486. doi:10.1111/bre.12330

Li, L., Fan, M., Davila, N., Jesmok, G., Mitsunaga, B., Tripati, A., et al. (2019). Carbonate Stable and Clumped Isotopic Evidence for Late Eocene Moderate to High Elevation of the East-central Tibetan Plateau and its Geodynamic Implications. *Geo. Soc. Am. Bull.* 131, 831–844. doi:10.1130/B32060.1

Li, S. H., Ji, X. P., Harrison, T., Deng, C. L., Wang, S. Q., Wang, L. R., et al. (2020a). Uplift of the Hengduan Mountains on the southeastern Margin of the Tibetan Plateau in the Late Miocene and its Paleoenvironmental Impact on Hominoid Diversity. *Palaeogeogr. Palaeoclimatol. Palaeoecol.* 553. doi:10.1016/j.palaeo.2020.109794

Li, S. H., van Hinsbergen, D. J. J., Najman, Y., Liu-Zeng, J., Deng, C. L., and Zhu, R. X. (2020b). Does Pulsed Tibetan Deformation Correlate with Indian Plate Motion Changes? *Earth Planet. Sci. Lett.* 536, 116144. doi:10.1016/j.epsl.2020.116144

Lin, J., Dai, J. G., Zhuang, G. S., Jia, G. D., Zhang, L. M., Ning, Z. J., et al. (2020). Late Eocene-Oligocene High Relief Paleotopography in the north central Tibetan Plateau: Insights from Detrital Zircon U-Pb Geochronology and Leaf Wax Hydrogen Isotope Studies. *Tectonics* 39, e2019TC005815. doi:10.1029/2019TC005815

Liu, H., Yang, H., Cao, Y. N., and Liu, W. G. (2018). Compound-specific δD and its Hydrological and Environmental Implication in the Lakes on the Tibetan Plateau. *Sci. China Earth Sci.* 61, 765–777. doi:10.1007/s11430-017-9182-2

Liu, W. G., Yang, H., Wang, H. Y., An, Z. S., Wang, Z., and Leng, Q. (2015). Carbon Isotope Composition of Long Chain Leaf Wax *N*-Alkanes in lake Sediments: A Dual Indicator of Paleoenvironment in the Qinghai-Tibet Plateau. *Org. Geochem.* 83–84, 190–201. doi:10.1016/j.orggeochem.2015.03.017

Luo, P., Peng, P. A., Lü, H. Y., Zheng, Z., and Wang, X. (2012). Latitudinal Variations of CPI Values of Long-Chain *N*-Alkanes in Surface Soils: Evidence for CPI as a Proxy of Aridity. *Sci. China Earth Sci.* 55, 1134–1146. doi:10.1007/s11430-012-4401-8

Meister, P., Reyes, C., Beaumont, W., Rincon, M., Collins, L., Berelson, W., et al. (2011). Calcium and Magnesium-limited Dolomite Precipitation at Deep Springs Lake, California. *Sedimentology* 58, 1810–1830. doi:10.1111/j.1365-3091.2011.01240.x

Meyers, P. A. (2003). Applications of Organic Geochemistry to Paleolimnological Reconstructions: A Summary of Examples from the Laurentian Great Lakes. *Org. Geochem.* 34, 261–289. doi:10.1016/S0146-6380(02)00168-7

Meyers, P., and Ishiwatari, R. (1993). Lacustrine Organic Geochemistry—An Overview of Indicators of Organic Matter Sources and Diagenesis in lake Sediments. *Org. Geochem.* 20, 876–900. doi:10.1016/0146-6380(93)90100-P

Miller, K. G., Browning, J. V., Schmelz, W. J., Kopp, R. E., Mountain, G. S., and Wright, J. D. (2020). Cenozoic Sea-Level and Cryospheric Evolution from Deep-Sea Geochemical and continental Margin Records. *Sci. Adv.* 6. eaaz1346. doi:10.1126/sciadv.aaz1346

Moldowan, J. M., Peters, K. E., and Walters, C. C. (2005). *The Biomarker Guide: Biomarkers and Isotopes in Petroleum Systems and Earth History*. Cambridge: Cambridge University Press.

Nichols, J. E., Booth, R. K., Jackson, S. T., Pendall, E. G., and Huang, Y. (2006). Paleohydrologic Reconstruction Based on *N*-Alkane Distributions in Ombrotrophic Peat. *Org. Geochem.* 37, 1505–1513. doi:10.1016/j.orggeochem.2006.06.020

Ogg, J., and Bardot, L. (2001). "Aptian through Eocene Magnetostratigraphic Correlation of the Blake Nose Transect (Leg 171B), Florida continental Margin," in *Proceedings of the Ocean Drilling Program, Scientific Results*. Editors D. Kroon, R. D. Norris, and A. Klaus (College Station: Ocean Drilling Program). [Texas]. doi:10.2973/odp.proc.sr.171b.104.2001

Ouyang, X., Guo, F., and Bu, H. (2015). Lipid Biomarkers and Pertinent Indices from Aquatic Environment Record Paleoclimate and Paleoenvironment Changes. *Quat. Sci. Rev.* 123, 180–192. doi:10.1016/j.quascirev.2015.06.029

Peters, K. E., Moldowan, J. M., and Walters, C. (2007). *The Biomarker Guide: Biomarkers and Isotopes in Petroleum Systems and Earth History*. Cambridge: Cambridge University Press.

Poynter, J. G., Farrimond, P., Robinson, N., and Eglinton, G. (1989). Aeolian-Derived Higher Plant Lipids in the Marine Sedimentary Record: Links with

Palaeoclimate. *Paleoclimatology Paleometeorology: Mod. Past Patterns Glob. Atmos. Transport*, 435–462. doi:10.1007/978-94-009-0995-3_18

Pu, Y., Zhang, H. C., Wang, Y. L., Lei, G. L., Nace, T., and Zhang, S. P. (2011). Climatic and Environmental Implications from N-Alkanes in Glacially Eroded lake Sediments in Tibetan Plateau: An Example from Ximen Co. *Sci. Bull.* 56, 1503–1510. doi:10.1007/s11434-011-4454-7

QBGMR (Qinghai Bureau of Geology and Mineral Resources) (1991). *Regional Geology of Qinghai Province*. Beijing: Geological Publishing House, 1–662.

Rao, Z. G., Jia, G. D., Li, Y. X., Chen, J. H., Xu, Q. H., and Chen, F. H. (2016). Asynchronous Evolution of the Isotopic Composition and Amount of Precipitation in north China during the Holocene Revealed by a Record of Compound-specific Carbon and Hydrogen Isotopes of Long-Chain *N*-Alkanes from an alpine lake. *Earth Planet. Sci. Lett.* 446, 68–76. doi:10.1016/j.epsl.2016.04.027

Ratnayake, N. P., Suzuki, N., Okada, M., and Takagi, M. (2006). The Variations of Stable Carbon Isotope Ratio of Land Plant-Derived *N*-Alkanes in Deep-Sea Sediments from the Bering Sea and the North Pacific Ocean during the Last 250,000 Years. *Chem. Geol.* 228, 197–208. doi:10.1016/j.chemgeo.2005.10.005

Sachse, D., Billault, I., Bowen, G. J., Chikaraishi, Y., Dawson, T. E., Feakins, S. J., et al. (2012). Molecular Paleohydrology: Interpreting the Hydrogen-Isotopic Composition of Lipid Biomarkers from Photosynthesizing Organisms. *Ann. Rev. Earth Planet.* 40, 221–249. doi:10.1146/annurev-earth-042711-105535

Spurlin, M. S., Yin, A., Horton, B. K., Zhou, J. Y., and Wang, J. H. (2005). Structural Evolution of the Yushu-Nangqian Region and its Relationship to Syncolli-Sional Igneous Activity, East-central Tibet. *Geol. Soc. Am. Bull.* 117, 1293–1317. doi:10.1130/B25572.1

Suganuma, Y., and Ogg, J. (2006). "Campanian through Eocene Magnetostratigraphy of Sites 1257–1261, ODP Leg 207, Demerara Rise (Western Equatorial Atlantic)," in *Proceeding of the Ocean Drilling Program, Scientific Results*. Editors D. C. Mosher, J. Erbacher, and M. J. Malone (College Station: Ocean Drilling Program). [Texas].

Sun, J. M., Windley, B. F., Zhang, Z. L., Fu, B. H., and Li, S. H. (2016). Diachronous Seawater Retreat from the Southwestern Margin of the Tarim Basin in the Late Eocene. *J. Asian Earth Sci.* 116, 222–231. doi:10.1016/j.jseaes.2015.11.020

Sun, Y. Y., Liu, J., Liang, Y., Ji, J. L., Liu, W. G., Aitchison, J. C., et al. (2020). Cenozoic Moisture Fluctuations on the Northeastern Tibetan Plateau and Association with Global Climatic Conditions. *J. Asian Earth Sci.* 104490. doi:10.1016/j.jseaes.2020.104490

Tang, M. Y., Liu, Z. J., Hoke, G. D., Xu, Q., Wang, W. T., Li, Z. F., et al. (2017). Paleoelevation Reconstruction of the Paleocene–Eocene Gonjo basin, SE-central Tibet. *Tectonophysics.* 712–713, 170–181. doi:10.1016/j.tecto.2017.05.018

Wang, B. L., Liu, C. Q., Peng, X., and Wang, F. S. (2013). Mechanisms Controlling the Carbon Stable Isotope Composition of Phytoplankton in Karst Reservoirs. *J. Limnol.* 72, 11. doi:10.4081/jlimnol.2013.e11

Wang, C. S., Zhao, X. X., Liu, Z. F., Lippert, P. C., Graham, S. A., Coe, R. S., et al. (2008). Constraints on the Early Uplift History of the Tibetan Plateau. *Proc. Natl. Acad. Sci.* 105, 4987–4992. doi:10.1073/pnas.0703595105

Wang, G., Wang, Y. L., Wei, Z. F., He, W., Zhang, T., Ma, X. Y., et al. (2021b). Distribution of *N*-alkan-2-ones in Qionghai Lake Sediments, Southwest China, and its Potential for Late Quaternary Paleoclimate Reconstruction. *J. Quat. Sci.* 36, 288–297. doi:10.1002/jqs.3271

Wang, G., Wang, Y. L., Wei, Z. F., He, W., and Zhang, T. (2021a). Reconstruction of Temperature and Precipitation Spanning the Past 28 Kyr Based on Branched Tetraether Lipids from Qionghai Lake, Southwestern China. *Palaeogeogr. Palaeoclimat. Palaeoecol.* 562, 110094. doi:10.1016/j.palaeo.2020.110094

Wang, H. Y., Dong, H. L., Zhang, C. L., Jiang, H. C., and Liu, W. G. (2016). A 12-kyr Record of Microbial Branched and Isoprenoid Tetraether index in Lake Qinghai, Northeastern Qinghai-Tibet Plateau: Implications for Paleoclimate Reconstruction. *Sci. China Earth Sci.* 59, 951–960. doi:10.1007/s11430-015-5213-4

Wang, Y. L., Fang, X. M., Zhang, T. W., Li, Y. M., Wu, Y., He, D. X., et al. (2012). Distribution of Biomarkers in Lacustrine Sediments of the Linxia Basin, NE Tibetan Plateau, NW China: Significance for Climate Change. *Sediment. Geol.* 243-244, 108–116. doi:10.1016/j.sedgeo.2011.10.006

Warren, J. K. (2000). Dolomite: Occurrence, Evolution and Economically Important Associations. *Earth-sci. Rev.* 52, 1–81. doi:10.1016/S0012-8252(00)00022-2

Warren, J. K. (2006). *Evaporites: Sediments, Resources and Hydrocarbons*. Berlin: Springer.

Wei, Y. L., and Han, F. X. (2015). Climate Change Characteristics of Nangqian County during 1961~2013. *Qinghai Agric. For. Tech.* 1, 39–44. (in Chinese with English asbtract). doi:10.3969/j.issn.1004-9967.2015.01.012

Westerhold, T., Marwan, N., Drury, A. J., Liebrand, D., Agnini, C., Anagnostou, E., et al. (2020). An Astronomically Dated Record of Earth's Climate and its Predictability over the Last 66 Million Years. *Science* 369. doi:10.1126/science.aba6853

Wu, M. H., Zhuang, G. S., Hou, M. Q., and Liu, Z. H. (2021). Expanded Lacustrine Sedimentation in the Qaidam Basin on the Northern Tibetan Plateau: Manifestation of Climatic Wetting during the Oligocene Icehouse. *Earth Planet. Sci. Lett.* 565, 116935. doi:10.1016/j.epsl.2021.116935

Xiong, Y., and Li, C. K. (1990). *Soils of China*. Beijing: Science Press, 590. (in Chinese with English abstract).

Xiong, Z. Y., Ding, L., Spicer, R. A., Farnsworth, A., Wang, X., Valdes, P., et al. (2020). The Early Eocene Rise of the Gonjo Basin, SE Tibet: from Low Desert to High Forest. *Earth Planet. Sci. Lett.* 543. doi:10.1016/j.epsl.2020.116312

Ye, C. C., Yang, Y. B., Fang, X. M., Hong, H. L., Zhang, W. L., Yang, R. S., et al. (2018). Mineralogical and Geochemical Discrimination of the Occurrence and Genesis of Palygorskite in Eocene Sediments on the Northeastern Tibetan Plateau. *Geochem. Geophys. Geosystems* 19, 567–581. doi:10.1002/2017GC007060

Yin, A., and Harrison, T. M. (2003). Geologic Evolution of the Himalayan-Tibetan Orogen. *Ann. Rev. Earth Planet.* 28, 211–280. doi:10.1146/annurev.earth.28.1.211

Yu, X. F., Lü, X. X., Meyers, P. A., and Huang, X. Y. (2021). Comparison of Molecular Distributions and Carbon and Hydrogen Isotope Compositions of *N*-Alkanes from Aquatic Plants in Shallow Freshwater Lakes along the Middle and Lower Reaches of the Yangtze River, China. *Org. Geochem.* 158, 104270. doi:10.1016/j.orggeochem.2021.104270

Yuan, Q., Barbolini, N., Rydin, C., Gao, D. L., Wei, H. C., Fan, Q. S., et al. (2020a). Aridification Signatures from Fossil Pollen Indicate a Drying Climate in East-central Tibet during the Late Eocene. *Clim. Past.* 16, 2255–2273. doi:10.5194/cp-16-2255-2020

Yuan, Q., Fan, Q. S., Wei, H. C., Qin, Z. J., Li, Q. K., Du, Y. S., et al. (2020b). The Sedimentary Environment of the Late Eocene Gypsum in Nangqian Basin, Qinghai Province. *J. Salt Lake Res.* 28, 69–77. (in Chinses with English abstract). doi:10.12119/j.yhyj.2020010099

Yuan, Q., Vajda, V., Li, Q. K., Fan, Q. S., Wei, H. C., Qin, Z. J., et al. (2017). A Late Eocene Palynological Record from the Nangqian Basin, Tibetan Plateau: Implications for Stratigraphy and Paleoclimate. *Palaeoworld* 26, 369–379. doi:10.1016/j.palwor.2016.10.003

Zachos, J. C., Dickens, G. R., and Zeebe, R. E. (2008). An Early Cenozoic Perspective on Greenhouse Warming and Carbon-Cycle Dynamics. *Nature* 451, 279–283. doi:10.1038/nature06588

Zhang, P. Y., Jiang, F. J., Zhu, C. X., Huang, R. D., Hu, T., Xu, T. W., et al. (2021). Gas Generation Potential and Characteristics of Oil-Prone Shale in the Saline Lacustrine Rifting Basins: A Case Study of the Dongpu Depression, Bohai Bay Basin. *Energy Fuel* 35, 2192–2208. doi:10.1021/acs.energyfuels.0c03965

Zhang, P. Y., Wang, Y. L., Zhang, X. J., Wei, Z. F., Wang, G., Zhang, T., et al. (2022). Carbon, Oxygen and Strontium Isotopic and Elemental Characteristics of the Cambrian Longwangmiao Formation in South China: Paleoenvironmental Significance and Implications for Carbon Isotope Excursions. *Gondwana. Res.* 106, 174–190. doi:10.1016/j.gr.2022.01.008

Zhang, W. L., Fang, X. M., Zhang, T., Song, C. H., and Yan, M. D. (2020). Eocene Rotation of the Northeastern central Tibetan Plateau Indicating Stepwise Compressions and Eastward Extrusions. *Geophys. Res. Lett.* 47. doi:10.1029/2020GL088989

Zhang, Y., Huang, W. T., Zhang, Y. Y., Poujol, M., Guillot, S., Roperch, P., et al. (2019). Detrital Zircon Provenance Comparison between the Paleocene-Eocene Nangqian-Xialaxiu and Gongjue Basins: New Insights for Cenozoic Paleogeographic Evolution of the Eastern Tibetan Plateau. *Palaeogeogr. Palaeoclimat. Palaeoecol.*, 109241. doi:10.1016/j.palaeo.2019.109241

Zhao, T. Y., Yuan, Q., Chen, J. B., An, F. Y., Lv, S., Sun, A. J., et al. (2020). Clay Mineral Assemblage Characteristics and Sedimentary Environmental Significance of Gypsum-bearing Strata in Gongjue Formation, Nangqian Basin. *J. Salt Lake Res.* 28, 25–32. (in Chinese with English abstract). doi:10.12119/j.yhyj.202001004

Zheng, Y. H., Zhou, W. J., Meyers, P. A., and Xie, S. C. (2007). Lipid Biomarkers in the Zoigê-Hongyuan Peat deposit: Indicators of Holocene Climate Changes in West China. *Org. Geochem.* 38, 1927–1940. doi:10.1016/j.orggeochem.2007.06.012

Zhu, C. X., Jiang, F. J., Zhang, P. Y., Hu, T., Liu, Y., Xu, T. W., et al. (2021). Identification of Effective Source Rocks in Different Sedimentary Environments and Evaluation of Hydrocarbon Resources Potential: A Case Study of Paleogene Source Rocks in the Dongpu Depression, Bohai Bay Basin. *J. Pet. Sci. Eng.* 201, 108477. doi:10.1016/j.petrol.2021.108477

Conflict of Interest: The authors declare that the research was conducted in the absence of any commercial or financial relationships that could be construed as a potential conflict of interest.

Publisher's Note: All claims expressed in this article are solely those of the authors and do not necessarily represent those of their affiliated organizations, or those of the publisher, the editors, and the reviewers. Any product that may be evaluated in this article, or claim that may be made by its manufacturer, is not guaranteed or endorsed by the publisher.